Distorted Pacific-North American Teleconnection at the Last Glacial Maximum

Yongyun Hu[1*], Yan Xia[1], Zhengyu Liu[1,2], Yuchen Wang[1], Zhengyao Lu[1], and Tao Wang[3]

[1]Laboratory for Climate and Ocean-Atmosphere Studies, Department of Atmospheric and

Oceanic Sciences, School of Physics, Peking University, Beijing 100871, China

[2]Atmospheric Science Program, Department of Geography, Ohio State University, Columbus,

OH, 43210, USA

[3]Nansen-Zhu International Research Centre, Institute of Atmospheric Physics, Chinese Academy

of Sciences, Beijing 100029, China

Corresponding author: Yongyun Hu, email: yyhu@pku.edu.cn

Abstract

The Pacific-North American (PNA) teleconnection is one of the most important climate modes in the present climate condition, and it enables climate variations in the tropical Pacific to exert significant impacts on North America. Here, we show climate simulations that the PNA teleconnection was largely distorted or broken at the Last Glacial Maximum (LGM). The distorted PNA is caused by a split of the westerly jet stream, which is ultimately forced by the thick and large Laurentide ice sheet at the LGM. Changes in the jet stream greatly alter the extratropical wave guide, distorting wave propagation from the North Pacific to North America. The distorted PNA suggests that climate variability in the tropical Pacific, notably, El Niño and Southern Oscillation (ENSO), would have little direct impact on North American climate at the LGM.

1 Introduction

The Pacific-Northern-American (PNA) teleconnection is the major atmospheric teleconnection mode that links climate variations from the tropical Pacific to North America for the present-day climate state (Horel and Wallace, 1981; Wallace and Gutzler, 1981). Especially, climate variability associated with El Niño and Southern Oscillation (ENSO) exerts great impacts on the North American climate through the PNA teleconnection (Henderson and Robinson, 1994; Lau, 1997; Leathers et al., 1991; Straus and Shukla, 2002). It is well known that the PNA is largely constrained by extratropical atmospheric flows, notably, the extratropical wave guide (Held, 1983; Held et al., 2002; Hoskins and Karoly, 1981; Jin and Hoskins, 1995). Thus, changes in extratropical atmospheric flows should alter the PNA under different climate conditions.

It has been shown that greenhouse warming leads to a strengthening and a shift of the PNA due to altered extratropical atmospheric flows (Allan et al., 2014; Chen et al., 2017). There has also been a large body of works that demonstrated significant differences in extratropical atmospheric circulations in cold climates, notably, the Last Glacial Maximum (LGM). It was shown that during the LGM the Aleutian low pressure system was enhanced in winter, the Pacific high pressure system was weakened in summer (Yanase and Abe-Ouchi, 2007; Yanase and Abe-Ouchi, 2010), the westerly jet shifted southward (Braconnot et al., 2007; Otto-Bliesner et al., 2006), and transient waves were weakened over the North Pacific and strengthened over the North Atlantic (Justino and Peltier, 2005; Justino et al., 2005). These works suggest that the PNA could be changed for different climate regimes. Therefore, a natural question is whether the PNA is also significantly altered due to atmospheric circulation changes at the LGM.

The LGM occurred between 23,000 and 19,000 years ago (Clark et al., 2009; Clark and Mix, 2002). One of the most significant climatic characteristics at LGM is the maximum expansion of mid-latitude ice sheets. Extensive ice sheets grew over North America and northwestern Europe, with the Laurentide ice sheet over North America, in particular, of an ice thickness of 3 to 4 kilometers (Marshall et al., 2002). Early simulations have shown that the thick and large Laurentide ice sheet forced a split of the extratropical westerly jet stream into the northern and southern branches (Cohmap, 1988; Kutzbach and Wright, 1985; Rind, 1987), and that the jet split leads to regional climate changes over the globe, especially over North America. Proxy records showed that there were more storms and precipitation associated with the southern branch, causing high lake levels and increased woodlands in the southwestern United States (Cohmap, 1988; Kutzbach and Wright, 1985).

Recent modeling studies showed that the Arctic Oscillation and storm tracks at LGM differ significantly from the present (Justino and Peltier, 2005; La îné et al., 2009; Li and Battisti, 2008; Lü et al., 2010; Rivière et al., 2010), and that the Laurentide ice sheet can also influence the Southern-Hemisphere atmospheric teleconnection and climate variability over West Antarctic (Jones et al., 2018). Therefore, it is possible that changed atmospheric circulations at LGM might also significantly alter the PNA and thus climate linkage between the tropical Pacific and North America.

In the present paper, using climate simulation results, we show that the PNA is largely distorted or even broken by the Laurentide ice sheet at LGM, and that ENSO had little direct impact on North American climates. We will also address how the PNA is altered by the Laurentide ice sheet.

2 Models and data

87   The simulation results from the Paleoclimate Modeling Intercomparison Project 2 (PMIP2)

88   (Braconnot et al., 2012; Braconnot et al., 2007) and 3 (PMIP3) (Abe-Ouchi et al., 2015) are

89   utilized in this study. By comparing the PNA patterns in the Preindustrial condition (PIC) with

90   LGM simulations as well as our own sensitivity simulations, the changes in the PNA pattern at

91   LGM are identified. The horizonal resolution of the models we use are listed in table S1. For

92   comparison, we also use the NCEP/NCAR reanalysis data from 1988 to 2017 (Kistler et al.,

93   2001), with horizontal resolution of 2.5 °×2.5 °. We shall mainly focus on the simulation results

94   from the Community Climate System Model version 3 (CCSM3) (Collins et al., 2006; Jones et

95   al., 2018; Otto-Bliesner et al., 2006; Yeager et al., 2006), since our sensitivity simulations are

96   performed with the same model.

97   To understand the impact of the topography of the Northern-Hemisphere glacial ice sheets

98   on the PNA, we performed a series of sensitivity simulations with different ice sheet thicknesses,

99   which are 0%, 20%, 40%, 60%, 80%, 100%, and 150% of the ice sheet thickness that was used

100 in PMIP2. Note that different ice sheet reconstructions were used in PMIP2 and PMIP3

101 simulations. PMIP2 simulations used the ICE-5G (VM2) reconstruction (Peltier, 2004), while

102 PMIP3 simulations used the ICE-6G reconstruction. In general, the ice sheet thickness in ICE-

103 6G reconstruction is approximately equal to 80% of ICE-5G for most parts of the North

104 American region (Figure S1). In our sensitivity simulations, the case of 0% ice sheet thickness

105 means that the thickness of the ice sheet is set to zero, but the surface albedo remains ice albedo.

106 All other conditions are the same as that in the LGM simulations of PMIP2. The model for our

107 sensitivity simulations is a lower-resolution version of CCSM3 (T31), with horizontal a

108 resolution of 3.8 °×3.8 °. It differs from the PMIP2 models (T42), with a horizontal resolution of

109 2.8 °×2.8 °. Although the horizontal resolution in CCSM3 T31 is lower, it can well reproduce the

present-day PNA pattern in the PIC simulation, consistent with the results in Magnusdottir and Haynes (1999) and Löfverström et al. (2016). Therefore, the results here are not sensitive to model resolutions.

Following Horel and Wallace (1981) and Wallace and Gutzler (1981), the PNA teleconnection is characterized by the pointwise correlation method. The four base points that represent the centers of action are located near Hawaii (20 °N, 160 °W), North Pacific (45 °N, 165 °W), Alberta (55 °N, 115 °W), and the Gulf Coast (30 °N, 85 °W), respectively. The four base points were objectively derived with teleconnectivity analysis (Sherriff-Tadano and Itoh, 2013; Wallace and Gutzler, 1981). To examine whether models can reasonably simulate the PNA in PIC simulations and whether the PNA pathway is altered in LGM simulations, we loosely define a circular region around each of the centers of North Pacific, North America and the Gulf Coast (the base point is near Hawaii), with a radius of 10 degrees. For PIC simulations, if a model cannot generate statistically significant correlations (coefficients greater than 0.35) within the circular regions, the model is considered to have poor performance in simulating PNA. For these models with good performance in simulating PNA their PIC simulations, if their LGM simulations shows absence of significant correlations in the three circular regions, the PNA pathway is considered to be distorted or broken at LGM. Because the PNA is most active in DJF, our analysis below will mainly focus on the December-January-February (DJF) season.

In the present paper, all correlation analyses are conducted with monthly-mean model outputs of the last 30-year simulations. Correlation coefficient 0.35 corresponds to the 95% confidence level for 30-year correlations.

3 Results

Fig. 1 shows one-point correlation maps of 500 hPa geopotential heights in DJF, with the

base point near Hawaii. The correlation maps in Figs. 1a and 1b exhibit similar wave-train

patterns, with centers of positive and negative correlations extending from Hawaii to North

Pacific, Alberta, and finally to the Gulf Coast, respectively. Hence, the present-day PNA is

reproduced reasonably well in CCSM3. In contrast, this PNA pattern is altered dramatically in

the LGM simulation of CCSM3 (Fig. 1c). The negative correlation over North Pacific is reduced,

and the center of positive correlation is rather weak and shifted to the Arctic. The most striking

feature in Fig. 1c is that the center of negative correlation near the Gulf Coast completely

disappears. The results in Fig. 1 indicate that the PNA teleconnection is largely distorted at

LGM. This is the most important point of the present paper.
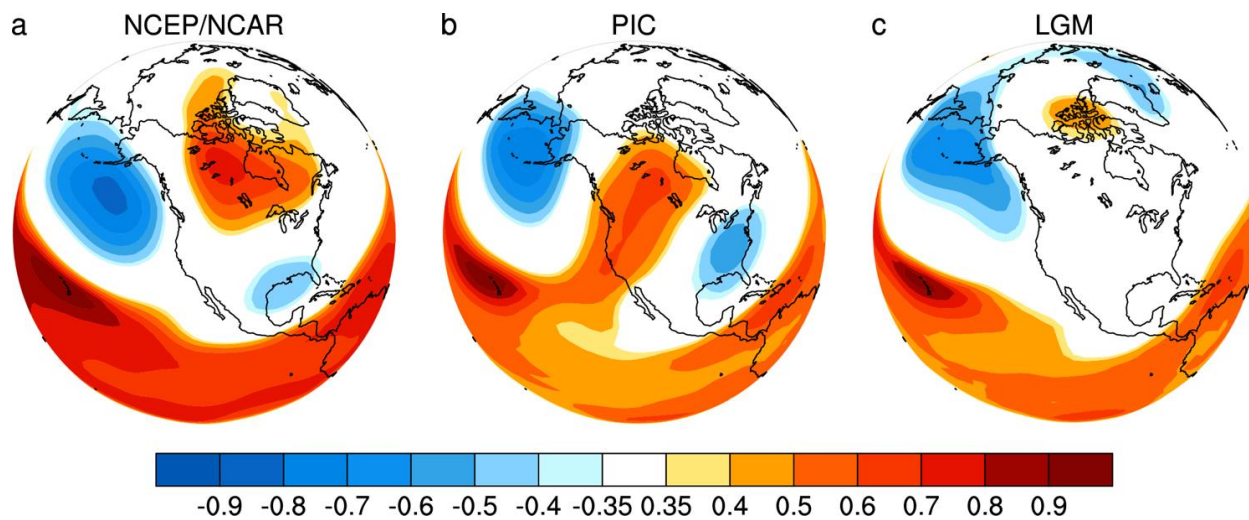
Fig. 1. One-point correlation maps of 500 hPa geopotential heights in DJF in NCEP/NCAR
reanalysis and PMIP2 CCSM3 simulations. (a) NCEP/NCAR, (b) PIC, and (c) LGM. The base
point is near Hawaii. The correlation coefficient of 0.35 corresponds to the 95% confidence level
for 30-year correlations.

This distorted PNA at LGM can also be seen from correlation maps for the other three base

points. When the base point is located over North Pacific (Fig. S2c), the center of positive

correlation over North America is shifted to northern Canada. For the base point over North

150   America (Fig. S2f), the negative correlations over North Pacific and the Gulf Coast are all

151   largely reduced, and the center of positive correlation near Hawaii disappears. This result

152   indicates a disconnection between North America and the tropical Pacific. For the base point

153   near the Gulf Coast (Fig. S2i), a wave train is established from North Pacific to the Gulf Coast,

154   while the center of positive correlation over North America is largely reduced, and the center of

155   positive correlation near Hawaii is absent.

156   The PNA teleconnection at LGM is even completely broken in other PMIP2 models. There

157   are seven PMIP2 models that have simulations available online. According to our definition,

158   CCSM3, ECBILTCLIO, HadCM3M2, and CNRM-CM33 can reasonably reproduce the PNA in

159   their PIC simulations (Fig. 1b and Figs. S3a-c), whereas IPSL-CM4-V1-MR, FGOALS-1.0g,

160   and MIROC3.2 have poor performance. In LGM simulations, the center of negative correlation

161   over North Pacific still exists in ECBILTCLIO, HadCM3M2, and CNRM-CM33 (Figs. S3d-f),

162   although they all shift away from the North Pacific base point and are largely reduced. However,

163   the center of positive correlation over North America completely disappears in these plots.

164   Moreover, the center of negative correlation near the Gulf Coast also disappears in the three

165   models.

166   PMIP3 simulations are also used to demonstrate the changes in the PNA teleconnection at

167   LGM. There are eight PMIP3 models that have LGM simulations available online. Again,

168   according to our definition, CCSM4, MRI-CGCM3, and MIROC-ESM can reasonably reproduce

169   the PNA in their PIC simulations (Figs. S4a-c). The LGM simulations of CCSM4 and MRI-

170   CGCM3 show the absence of the center of positive correlation over North America (Figs. S4d

171   and e). The center of positive correlation in MIROC-ESM is weak and biased toward the Arctic

172   (Fig. S4f). The center of negative correlation near the Gulf Coast is absent in MRI-CGCM3 and

173   MIROC-ESM. Although there is a negative center in CCSM4 (Fig. S4d), it is more like a result

174   of the subtropical wave train, rather than a part of PNA. Thus, the LGM simulations in PMIP3

175   models demonstrate that the PNA is either distorted or completely broken.

176   We have also done Empirical Orthogonal Function (EOF) and rotated EOF (REOF) analysis

177   to examine the PNA pattern for both LGM and PIC simulations (figures not shown here). It is

178   found that the second REOF modes in both the NCEP reanalysis and the CCSM3 PIC simulation

179   all well represent the loading pattern of the present-day PNA. However, the second REOF in the

180   CCSM3 LGM simulation does not show the PNA pattern. The third and fourth REOFs in the

181   LGM simulation show teleconnections between North Pacific and Arctic as well as between

182   North Pacific and the southern part of North America.

183   Fig. 2 illustrates PNA responses to different ice sheet thicknesses in sensitivity simulations.

184   The PNA pattern remains for ice sheet thicknesses no more than 60% of that in PMIP2 (Figs. 2a-

185   d). In contrast, the PNA is distorted as ice sheet thickness is increased to 80%. The center of

186   positive correlation is shifted to the Arctic, and the center of negative correlation near the Gulf

187   Coast disappears (Fig. 2e). As ice sheet thickness is further increased to 100 % and 150% (Figs.

188   2f-g), the center of positive correlation over North America disappears. Again, the center of

189   negative correlation is more like a part of the subtropical wave train. These results of sensitivity

190   simulations suggest that the PNA is distorted or even broken as the Laurentide ice sheet is

191   sufficiently thick.
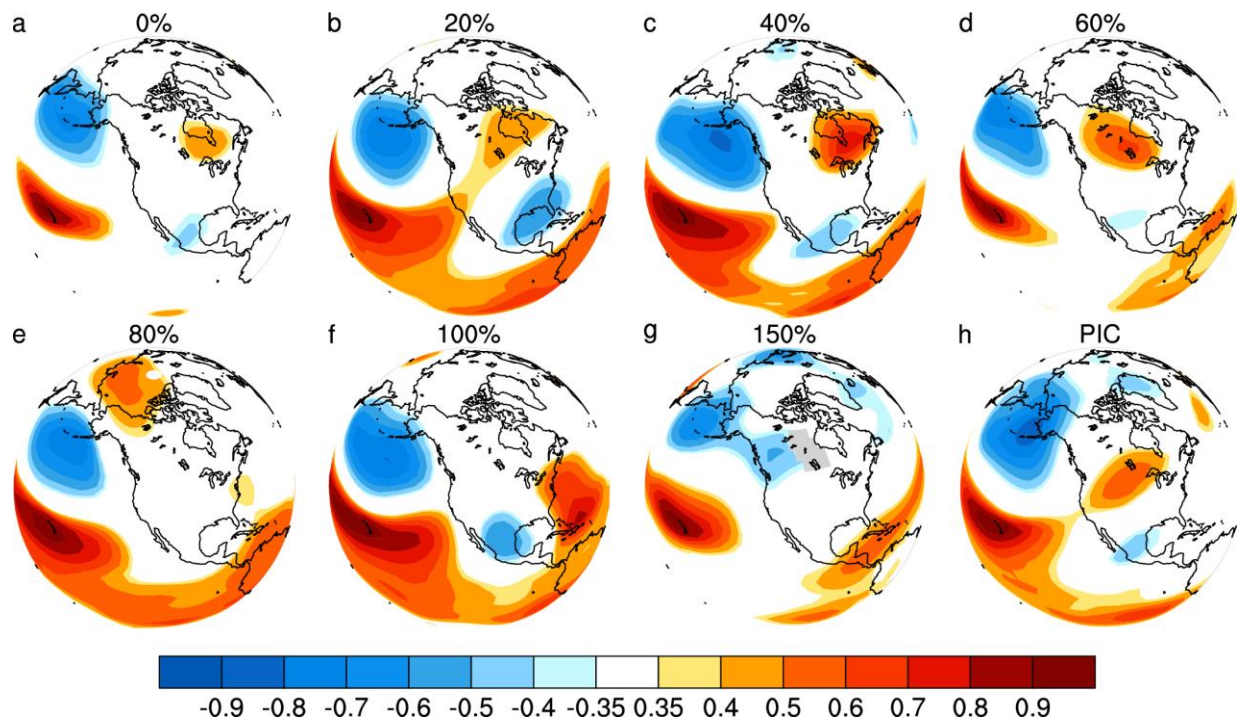
Fig. 2. One-point correlation maps of 500 hPa geopotential heights in DJF in sensitivity simulations, with different ice sheet thicknesses. The base point is near Hawaii. (a) 0%, (b) 20%. (c) 40%, (d) 60%, (e) 80%, (f) 100%, (g) 150%, and (h) PIC. The correlation coefficient of 0.35 corresponds to the 95% confidence level for 30-year correlations.

Fig. 3 summarizes correlation coefficients around the four base points for PMIP2, PMIP3, and our sensitivity simulations, according to our definition above. In Fig. 3a, both CCSM3 and CCSM4 show statistically significant correlations at all the four points in the PIC simulations. In contrast, they all demonstrate insignificant correlations near Alberta in LGM simulations. The significant correlation of CCSM4 LGM simulation near the Gulf coast is a result of subtropical wave train (Fig. S4d), as mentioned above. In Fig. 3b, the correlation coefficient near Alberta becomes less significant as ice sheet thickness reaches 80%. Correlation coefficients at the Gulf coast are insignificant for 80% and 150% ice sheet thickness. The significant correlation for 100% ice sheet thickness is a result of subtropical wave train, as shown in Fig. 2f.

207
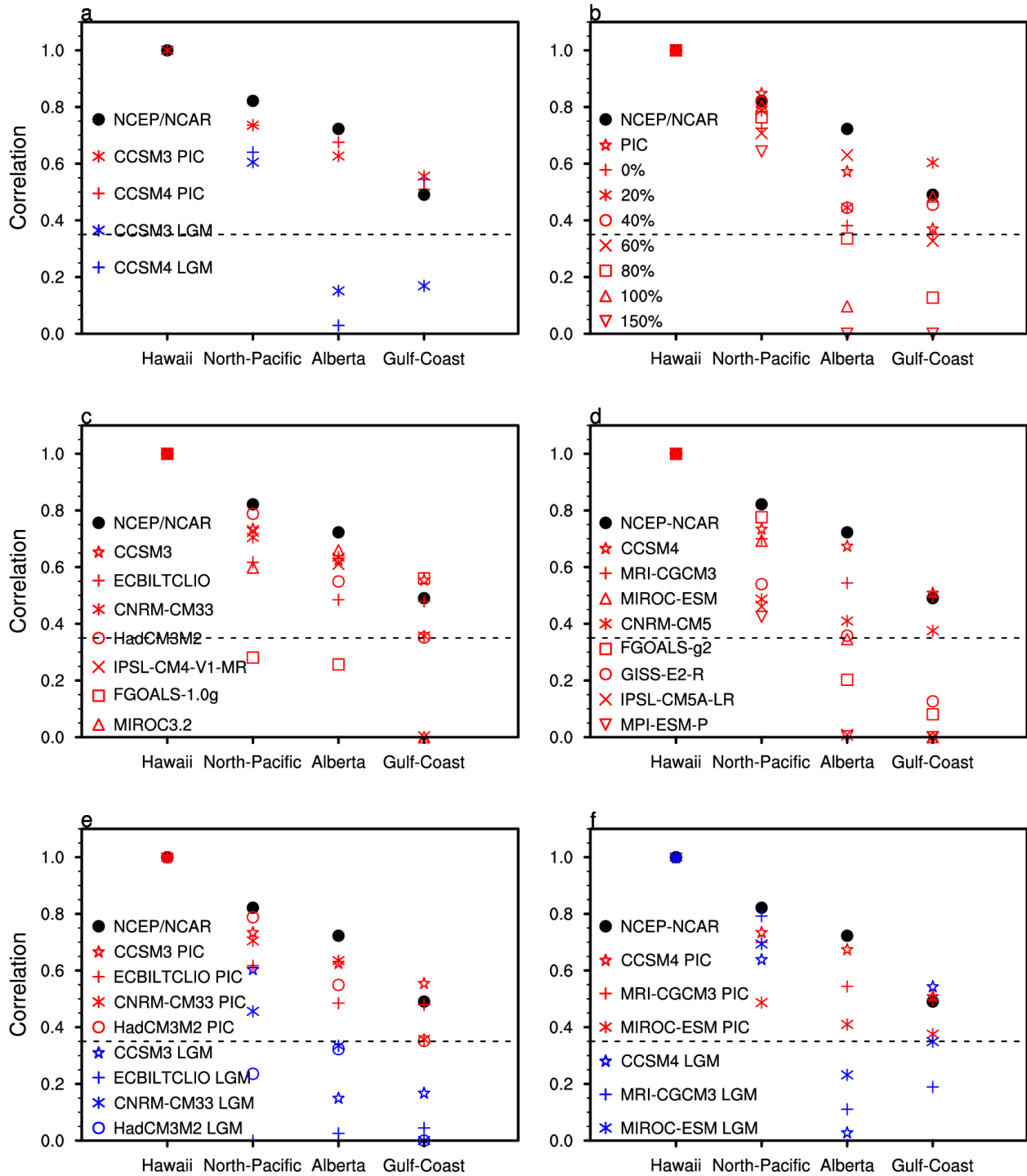
Fig. 3. Correlation coefficients at the four PNA action centers in PIC and LGM simulations for PMIP2 and PMIP3 models, with the base point near Hawaii. The negative values over North Pacific and the Gulf Coast are reversed to positive. The dashed lines correspond to 0.35, which represent the 95% confidence level. (a) CCSM3 and CCSM4, (b) sensitivity simulations, (c) PIC simulations of PMIP2 models, (d) PIC simulations of PMIP3 models, (e) LGM and PIC

213 simulations for well-performing PMIP2 models, and (f) LGM and PIC simulations for well-
214 performing PMIP3 models.

215

216   Figs. 3c and d shows that most PMIP2 and PMIP3 models are able to reproduce the

217 center of negative correlations over the North Pacific in their PIC simulations, except for

218 FGOALS-1.0g. FGOALS-1.0g that generates insignificant correlations at either North Pacific or

219 Alberta. CNRM-CM33 and MIROC3.2 cannot generate significant correlations near the Gulf

220 coast. Fig. 3d shows that CCSM4, MRI-CGCM3, and MIROC-ESM are able to reproduce

221 significant correlations at all four points in their PIC simulations, whereas the other 5 models

222 have insignificant correlations at either Alberta or the Gulf Coast. Figs. 3e and f show that

223 PMIP2 and PMIP3 models, which have good performance in simulating the PNA teleconnection

224 in PIC simulations, all cannot reproduce significant positive correlations at Alberta or even

225 negative correlations near the Gulf coast in the LGM simulations. These results all suggest that

226 the PNA was distorted or broken at LGM.

227   Because the PNA pattern is characterized by a quasi-stationary wave train from the

228 tropical Pacific to North America, the above simulation results suggest that the PNA wave-train

229 propagation is largely altered at LGM. This can be confirmed by activity fluxes of stationary

230 waves at 500 hPa calculated, using equation 7.1 in Plumb (1985) (Fig. 4), which represents the

231 propagation direction of stationary waves (Plumb, 1985). At present, the wave activity fluxes

232 have two branches for wave propagation from the North Pacific toward North America (Fig. 4a).

233 The major branch propagates northeastward, forming the PNA teleconnection, while the minor

234 branch propagates southeastward. At LGM, however, wave propagation is altered drastically.

235 Wave propagation is deflected toward the subtropics (Figs. 4b and c). This is consistent with the

236 correlation map in Fig. S2i that shows a wave train from North Pacific to the Gulf Coast.

237 Therefore, the distorted or broken PNA at LGM is mainly due to the deflection of wave

238 propagation toward the southeast.
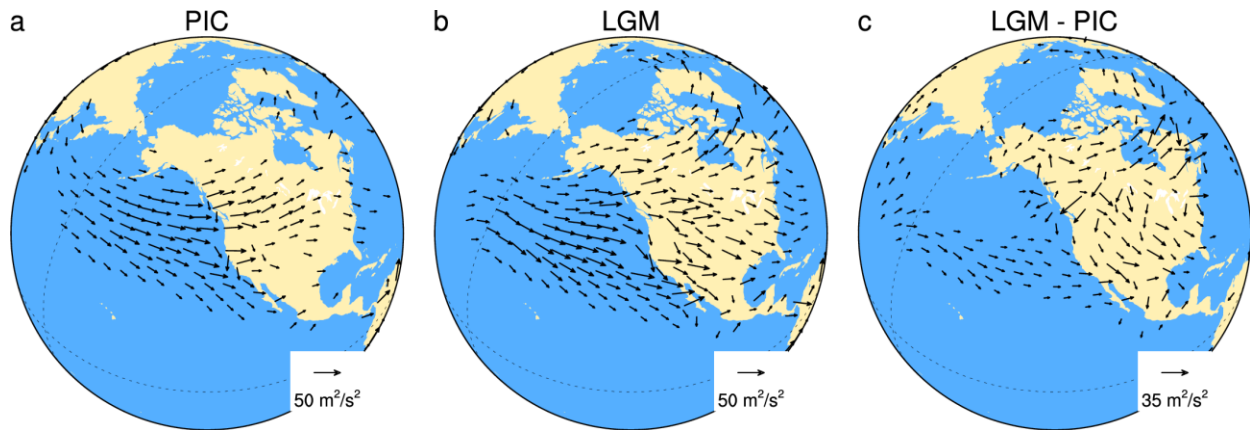
240 **Fig. 4.** Stationary wave activity fluxes in PMIP2 CCSM3 simulations at 500 hPa. (a) PIC, (b)
241 LGM, and (c) LGM – PIC. Length scales of wave activity vectors are marked in plots. Wave
242 activity vectors are plotted as their length scales are greater than 12 $m^2 s^{-2}$ in plots (a) and (b) and
243 6.5 $m^2 s^{-2}$ in plot (c). Here, stationary wave activity fluxes are calculated with monthly-mean
244 data.

245   Wave propagation is oriented by the extratropical wave guide, which in turn is

246 determined by extratropical zonal flows (Hoskins and Karoly, 1981; Jin and Hoskins, 1995).

247 Therefore, the deflection of stationary wave propagation at LGM is caused due to changes in

248 extratropical zonal flows. A comparison of zonal winds between PIC and LGM simulations

249 shows several major differences (Figs. 5a vs. 5b). First, the zonal jet stream is much stronger at

250 LGM than at present. Second, the jet is shifted equatorward at LGM, and the jet is turned

251 southeastward as it approaches the North American continent, in contrast to the northeast

252 orientation at present. Third, similar to that in early studies (Cohmap, 1988; Kutzbach and

253 Wright, 1985; Rind, 1987), the jet splits over North America with the much stronger branch

254 located in the subtropics, leaving the much weaker branch over northern Canada. These features

255 can be seen more clearly in differences of zonal winds between LGM and PIC simulations (Fig.

256 5c).

257
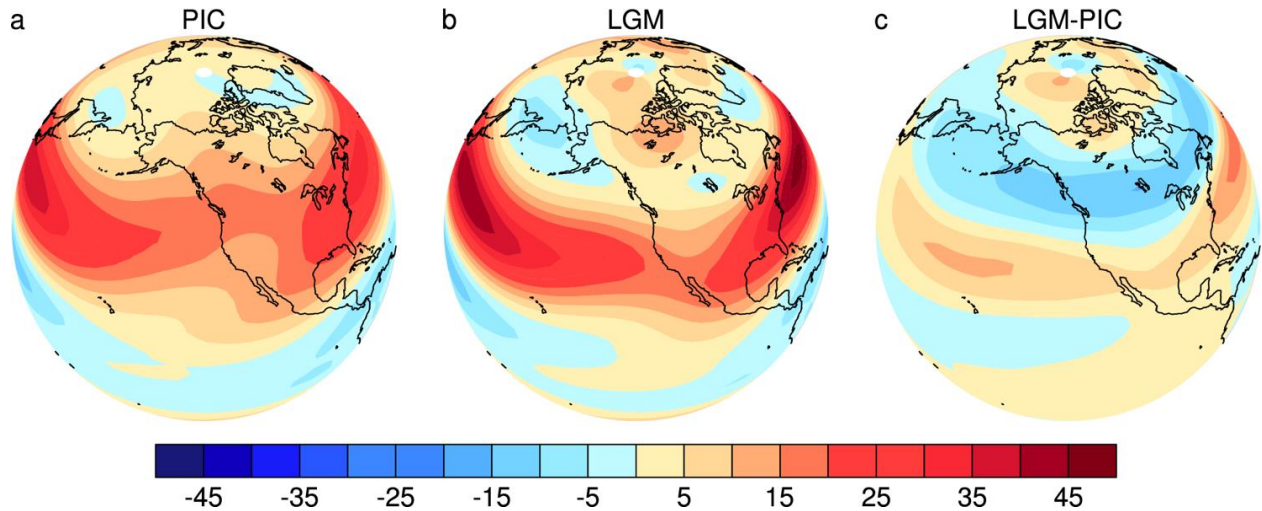
Fig. 5. Maps of 500 hPa zonal winds in DJF in PMIP2 CCSM3 simulations. (a) PIC, (b) LGM, and (c) LGM – PIC. Color interval: 5 m s^{-1}.

Differences of zonal winds over North America can also be illustrated with the vertical cross-sections along 100 °W (Fig. 6). The single subtropical westerly jet in the PIC simulation (Fig. 6b) is split into two jets at LGM (Fig. 6c): a subtropical jet at 30 °N and 200 hPa, and a subpolar jet at 63 °N and between 400 and 300 hPa. The subtropical jet is intensified to a maximum wind speed of 40 m s^{-1} and is located at a lower latitude, and it is much stronger than that in the PIC simulation (~ 30 m s^{-1}). The subpolar jet is much weaker, with a maximum speed of about 12 m s^{-1}. The differences in zonal winds are associated with different thermal structures between LGM and PIC simulations. Comparison of Figs. 6f with 6e shows that latitudinal temperature gradients in the subtropics are sharper at LGM than at present. Thus, the stronger subtropical jet is associated with the sharper temperature gradient.
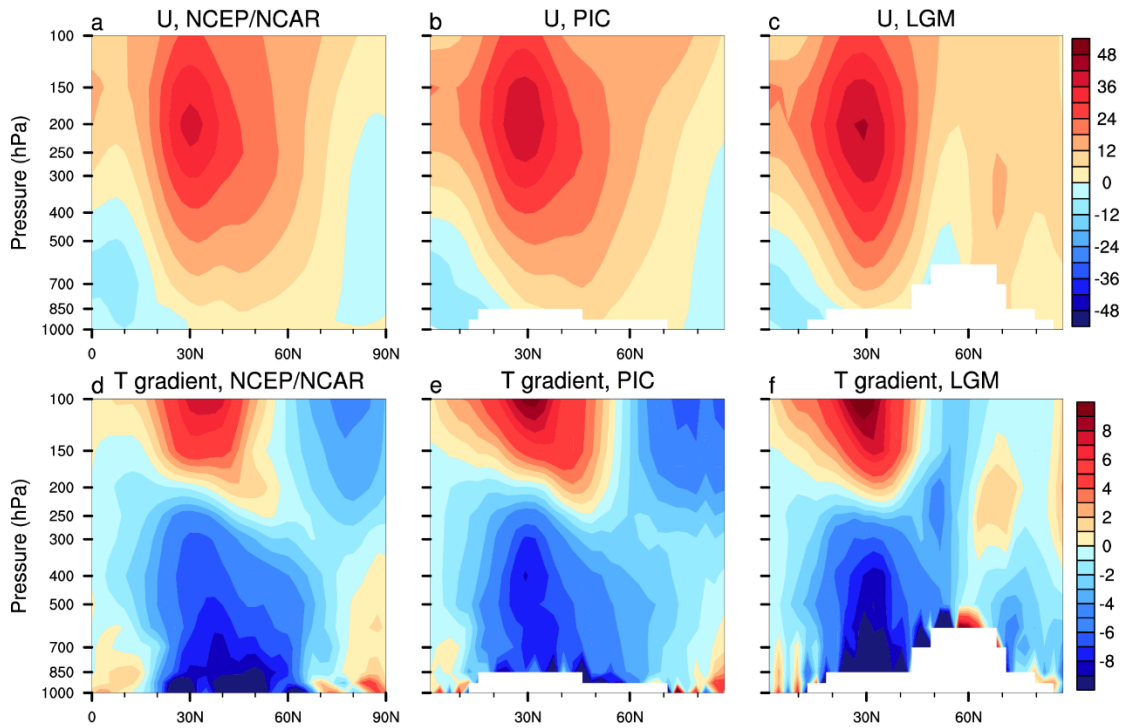
Fig. 6. Vertical cross sections of DJF zonal winds and meridional temperature gradients along the longitude of 100 °W in the NCEP/NCAR reanalysis and PMIP2 CCSM3 simulations. Top panels: zonal winds, and bottom panels: temperature gradients. Left panels: NCEP/NCAR, middle panels: PIC, and right panels: LGM. Zonal-wind unit is ms-1, and temperature gradient unit is K/(1000 km).

The jet split and the equatorward shift of the major jet branch are caused by the orographic forcing of the large and thick Laurentide ice sheet. Fig. S5 shows how the westerly jet responds to the ice sheet thickness in the sensitivity simulations. In the case with 0% ice sheet thickness, there is only a single jet in the subtropics (Fig. S5a), almost the same as that in the PIC simulation. As ice sheet thickness is increased, the jet is strengthened associated with the sharper meridional temperature gradient (Fig. S6), and the core of the jet becomes narrower. Significant jet splitting occurs as ice sheet thickness reaches 80% (Fig. S5e). It is the reason why the distortion of the PNA occurs as ice sheet thickness reaches 80%. As the ice sheet thickness is increased to 100% and 150%, the jet split becomes more significant, and easterly winds begin to develop over the ice sheet.

288   Note that the orographic forcing is further reinforced by the thermal forcing of the large ice

289   sheet (Liakka, 2012). The high albedo of the ice sheet causes cold air aloft, resulting in sharper

290   latitudinal temperature gradients in the subtropics at LGM. Thus, this enhanced temperature

291   gradient causes a stronger subtropical jet through the thermal wind relation. Our sensitivity

292   simulations also show that subtropical temperature gradients become sharper with increasing ice

293   sheet thicknesses.

294   The split of the westerly jet acts as wave guides to orient wave propagation, as shown in Fig.

295   4. The major path of wave propagation is associated with the major jet branch. Both Figs. S2c

296   and S2i all show that a southern wave train is established along the southern jet branch from

297   North Pacific sweeping across the southern US. This wave train would lead to more storms and

298   precipitation in the American Southwest, consistent with proxy records and previous modeling

299   studies (Cohmap, 1988). The minor path of wave propagation toward the Arctic is along with the

300   northern branch (Fig. 1c), but of a much reduced strength. As such, a southern wave guide is

301   established along the subtropical jet, while the northern wave guide is either distorted toward the

302   Arctic or completely broken.

303   Our sensitivity simulations demonstrate dramatic changes in the PNA wave train between

304   80% and 100% ice sheet thicknesses (Fig. 2e vs. Fig. 2f). The dramatic changes are associated

305   with the occurrence of easterly winds over the Laurentide ice sheet (Figs. 7a-c). For the case of

306   80% ice sheet thickness, westerly winds remain between the two jet streams (Fig. 7b). In

307   contrast, easterly winds appear over the ice sheet as the ice sheet thickness is increased to 100%

308   (Fig. 7c). The zero-wind line between easterly and westerly winds acts as the critical layer to

309   reflect stationary waves (Held, 1983). This can be addressed with calculations of critical

310   stationary wavenumbers (Fig. 7 d-f) (eq. 6.29 in Held (1983)). The orange-red shading indicates

311   the areas where stationary waves can propagate, while the shallow-blue shading indicates the

312   areas with imaginary wavenumbers, in which propagation of stationary waves is prohibited.

313   These shallow-blue areas are associated with the easterly winds. When the ice sheet thickness is

314   60% (Fig. 7d), North Pacific and North America are dominated with positive wavenumbers, and

315   the PNA remains. For 80% ice sheet thickness, imaginary wavenumbers occur in Northeast

316   Pacific and North America (Fig. 7e), and it forces the PNA wave train distorted toward the

317   Arctic. For 100% ice sheet thickness, the subpolar region is dominated with imaginary

318   wavenumbers (Fig. 7f). It causes stationary waves reflected southeastward, leading to the

319   establishment of the southern wave train and the breaking up of the northern wave train.

320
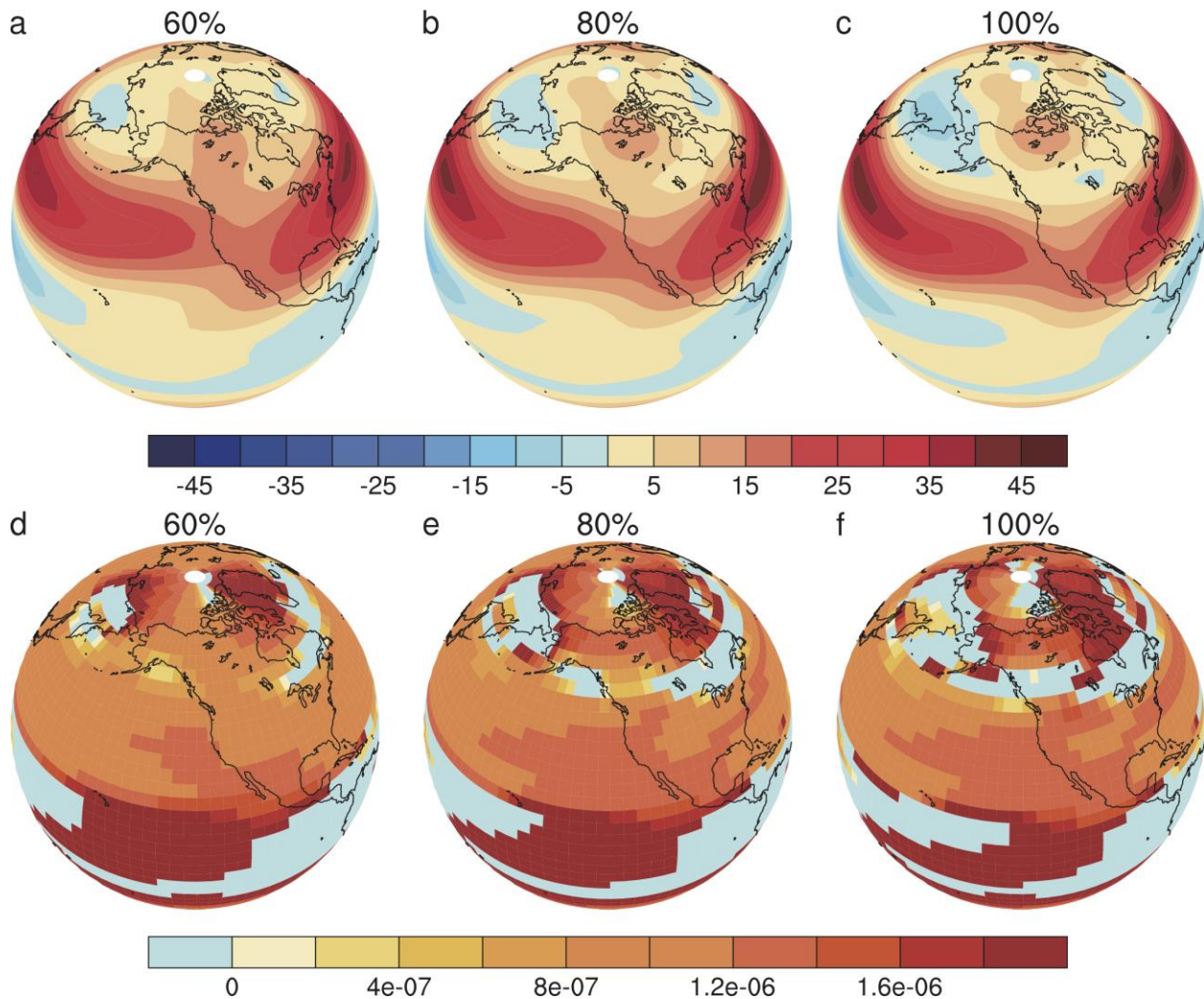
Fig. 7. Distributions of zonal winds and stationary wavenumbers for different ice sheet thicknesses in sensitivity simulations in DJF. Top panels: zonal winds, and bottom panels: stationary wavenumbers. (a, d) 60%, (b, e) 80%, and (c, f) 100%. Zonal-wind unit is m s^{-1}, and stationary wavenumber unit is m^{-1}. The shallow-blue areas in the bottom panels have imaginary wavenumbers.

The occurrence of easterly winds can be further illustrated with the geopotential heights at 500 hPa (Fig. 8). In both NCEP/NCAR reanalysis and the PIC simulation, there is only a weak ridge along the west coast of North America (Figs. 8a and b). In contrast, the ridge at LGM is largely enhanced and shows northwestern tilting (Fig. 8c). It is this strong ridge that leads to altered zonal flows. The major branch moves equatorward, and the minor branch flows around the ridge northward, resulting in the formation of easterly winds over the ice sheet and North Pacific. It also can be seen in the sensitivity simulations that the west-coast ridge increases with increasing ice sheet thickness (Fig. S7).
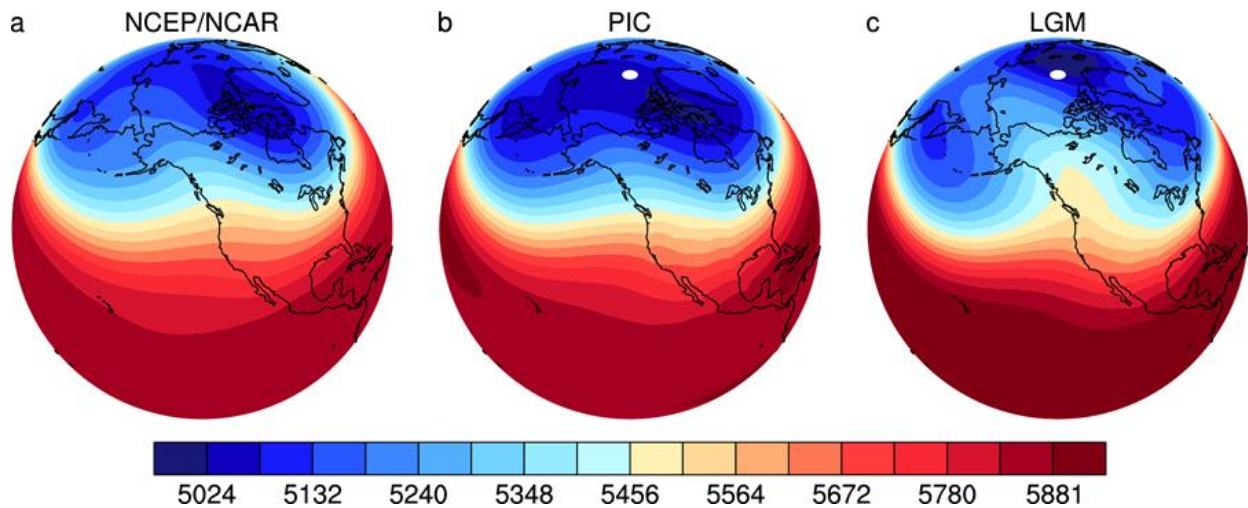
Fig. 8. Climatological mean 500 hPa geopotential heights in DJF in NCEP/NCAR reanalysis and PMIP2 CCSM3 simulations. (a) NCEP/NCAR, (b) PIC, and (c) LGM. The unit is meter.

The distorted or broken PNA teleconnection at LGM suggests a disconnection of climate variability from the tropical Pacific to the North American continent, such that ENSO would

341 have little direct influence on North American climates. Fig. 9 shows regression maps of surface

342 air temperatures (SATs) on the Nino3.4 index in DJF. At present, the remote ENSO impacts on

343 North American SATs through the PNA teleconnection can be identified clearly (Figs. 9a and

344 9b), which is characterized by an anomalously warm climate over the northwestern North

345 America and an anomalously cold climate over the southeastern United State. However, there are

346 no significant regressions of SATs over North America at LGM (Fig. 9c), except for the positive

347 values near the east coast.
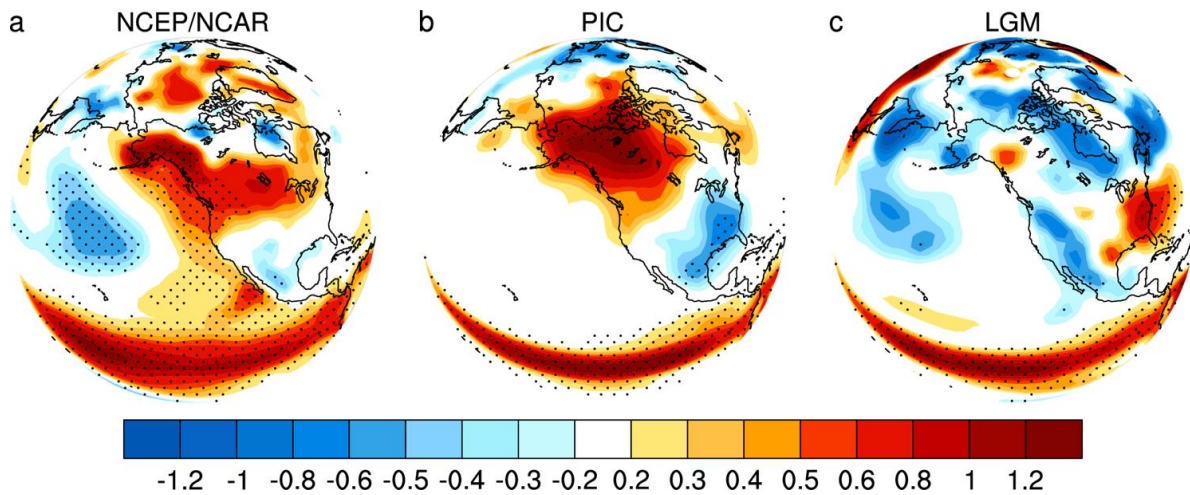
348

349 **Fig. 9.** DJF SAT regressions on the Nino3.4 index in NCEP/NCAR reanalysis and PMIP2
350 CCSM3 simulations. (a) NCEP/NCAR reanalysis, (b) PIC, and (c) LGM. The regression value
351 of 0.21 corresponds to the 95% confidence level for 30-year regressions.
352
353   At present, ENSO also has important influences on North American precipitation. Similar

354 features can also be seen from regression maps of precipitation (Fig. 10). Fig. 10a shows

355 precipitation regression on the Nino3.4 index in the PIC simulation. The wave train pattern of

356 precipitation is clearly shown in the plot. However, the wave train of precipitation is absent in

357 the LGM simulations (Fig. 10b).

358
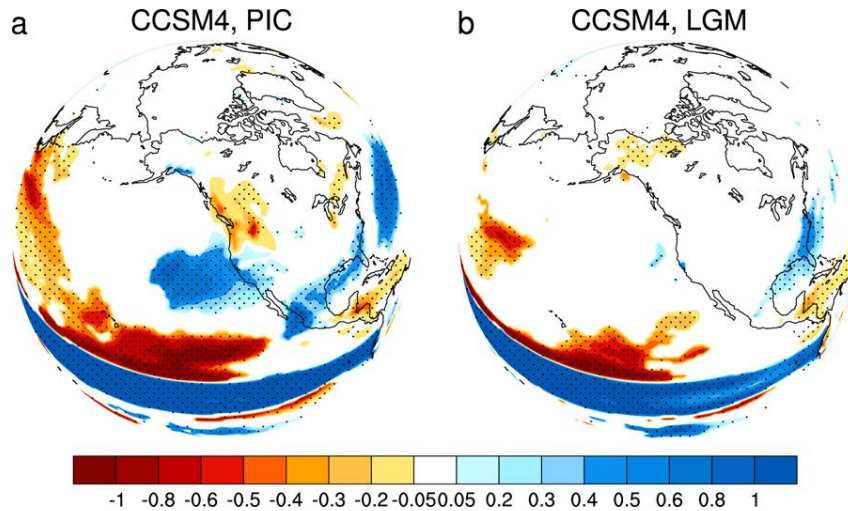
Fig. 10. Precipitation regressions on the Nino3.4 index in the CCSM4 PMIP3 simulations. (a) PIC, and (b) LGM. Dotted areas indicate significant regressions for the 95% confidence level for 30-year regressions.

4 Conclusions and Discussion

We have shown in climate simulations that the large and thick Laurentide ice sheet at LGM forced jet splitting and the formation of easterly winds over North America. It consequently causes altered wave guides and distorted or broken PNA. It appears that the PNA was separated into two teleconnections at LGM. One is from North Pacific to Arctic, and the other one is from North Pacific to the southern part of North America.

This result suggests that ENSO would have little direct influence on North American climates at LGM. Our study provides a dynamic framework to understand the PNA teleconnection not only at LGM but also in other glacial periods. This understanding may help us interpreting proxy records in the past. For example, a previous study on varve record in New England linked the change of the intensity of interannual variability in the northeastern US during the early glacial period to the change of ENSO intensity (Rittenour et al., 2000). Our study suggests that this interannual variability is unlikely to be caused by the climate variability

376 from the tropical Pacific, because of the distorted or broken PNA teleconnection; instead, it

377 reflects mainly the change of local climate variability (Liu et al., 2014). Much further work is

378 needed in developing proxy records of high temporal resolutions to identify the PNA change in

379 paleoclimate records.

380 Previous works have shown weaker ENSO variability at LGM (Merkel et al., 2010; Zhu

381 et al., 2017), and that the weaker ENSO leads to altered teleconnection patterns. How the weaker

382 tropical variability would impact climates over extratropics and high-latitudes, through the

383 altered atmospheric teleconnections, deserves future studies.

384

385 **Acknowledgements**

386 We thank the international modeling groups of the PMIP2 and PMIP3 projects who make

387 the simulation data available. We also thank modeling groups of CMIP3 and CMIP5 whose pre-

388 industry simulation data are used here. NCEP Reanalysis data are provided by the

389 NOAA/OAR/ESRL PSD, Boulder, Colorado, USA, from their Web site at

390 http://www.cdc.noaa.gov/. Y. Hu and Y. Xia are supported by the National Natural Science

391 Foundation of China (NSFC) under grants 41888101 and 41761144072, and Z. Liu is supported

392 by NSFC under grant 41630527. We thank the Editor and two anonymous reviewers for their

393 insightful comments on the paper.

References

Abe-Ouchi, A., Saito, F., Kageyama, M., Braconnot, P., Harrison, S. P., Lambeck, K., Otto-
    Bliesner, B. L., Peltier, W. R., Tarasov, L., Peterschmitt, J. Y., and Takahashi, K.: Ice-sheet
    configuration in the CMIP5/PMIP3 Last Glacial Maximum experiments, Geosci. Model
    Dev., 8, 3621-3637, 2015.

Allan, A. M., Hostetler, S. W., and Alder, J. R.: Analysis of the present and future winter Pacific-
    North American teleconnection in the ECHAM5 global and RegCM3 regional climate
    models, Climate Dynamics, 42, 1671-1682, 2014.

Braconnot, P., Harrison, S. P., Kageyama, M., Bartlein, P. J., Masson-Delmotte, V., Abe-Ouchi,
    A., Otto-Bliesner, B., and Zhao, Y.: Evaluation of climate models using palaeoclimatic data,
    Nature Climate Change, 2, 417, 2012.

Braconnot, P., Otto-Bliesner, B., Harrison, S., Joussaume, S., Peterchmitt, J. Y., Abe-Ouchi, A.,
    Crucifix, M., Driesschaert, E., Fichefet, T., Hewitt, C. D., Kageyama, M., Kitoh, A., Laîné,
    A., Loutre, M. F., Marti, O., Merkel, U., Ramstein, G., Valdes, P., Weber, S. L., Yu, Y., and
    Zhao, Y.: Results of PMIP2 coupled simulations of the Mid-Holocene and Last Glacial
    Maximum – Part 1: experiments and large-scale features, Clim. Past, 3, 261-277, 2007.

Chen, Z., Gan, B., Wu, L., and Jia, F.: Pacific-North American teleconnection and North Pacific
    Oscillation: historical simulation and future projection in CMIP5 models, Climate
    Dynamics, doi: 10.1007/s00382-017-3881-9, 2017. 2017.

Clark, P. U., Dyke, A. S., Shakun, J. D., Carlson, A. E., Clark, J., Wohlfarth, B., Mitrovica, J. X.,
    Hostetler, S. W., and McCabe, A. M.: The Last Glacial Maximum, Science, 325, 710-714,
    2009.

416 Clark, P. U. and Mix, A. C.: Ice sheets and sea level of the Last Glacial Maximum, Quaternary

417   Science Reviews, 21, 1-7, 2002.

418 Cohmap, M.: Climatic Changes of the Last 18,000 Years: Observations and Model Simulations,

419   Science, 241, 1043-1052, 1988.

420 Collins, W. D., Bitz, C. M., Blackmon, M. L., Bonan, G. B., Bretherton, C. S., Carton, J. A.,

421   Chang, P., Doney, S. C., Hack, J. J., Henderson, T. B., Kiehl, J. T., Large, W. G., McKenna,

422   D. S., Santer, B. D., and Smith, R. D.: The Community Climate System Model Version 3

423   (CCSM3), Journal of Climate, 19, 2122-2143, 2006.

424 Held, I. M.: Stationary and Quasi-stationary Eddies in the Extratropical Troposphere: Theory. In:

425   Large-scale Dynamical Processes in the Atmosphere, B. J. Hoskins and Pearce, R. P. (Eds.),

426   Academic Press, 1983.

427 Held, I. M., Ting, M., and Wang, H.: Northern Winter Stationary Waves: Theory and Modeling,

428   Journal of Climate, 15, 2125-2144, 2002.

429 Henderson, K. G. and Robinson, P. J.: Relationships between the pacific/north american

430   teleconnection patterns and precipitation events in the south‐eastern USA, International

431   Journal of Climatology, 14, 307-323, 1994.

432 Horel, J. D. and Wallace, J. M.: Planetary-Scale Atmospheric Phenomena Associated with the

433   Southern Oscillation, Monthly Weather Review, 109, 813-829, 1981.

434 Hoskins, B. J. and Karoly, D. J.: The Steady Linear Response of a Spherical Atmosphere to

435   Thermal and Orographic Forcing, Journal of the Atmospheric Sciences, 38, 1179-1196,

436   1981.

437 Jin, F. and Hoskins, B. J.: The Direct Response to Tropical Heating in a Baroclinic Atmosphere,

438   Journal of the Atmospheric Sciences, 52, 307-319, 1995.

439   Jones, T. R., Roberts, W. H. G., Steig, E. J., Cuffey, K. M., Markle, B. R., and White, J. W. C.:

440   Southern Hemisphere climate variability forced by Northern Hemisphere ice-sheet

441   topography, Nature, 554, 351, 2018.

442   Justino, F. and Peltier, W. R.: The glacial North Atlantic Oscillation, Geophysical Research

443   Letters, 32, 2005.

444   Justino, F., Timmermann, A., Merkel, U., and Souza, E. P.: Synoptic Reorganization of

445   Atmospheric Flow during the Last Glacial Maximum, Journal of Climate, 18, 2826-2846,

446   2005.

447   Kistler, R., Kalnay, E., Collins, W., Saha, S., White, G., Woollen, J., Chelliah, M., Ebisuzaki,

448   W., Kanamitsu, M., Kousky, V., van den Dool, H., Jenne, R., and Fiorino, M.: The NCEP-

449   NCAR 50-year reanalysis: Monthly means CD-ROM and documentation, B Am Meteorol

450   Soc, 82, 247-267, 2001.

451   Kutzbach, J. E. and Wright, H. E.: Simulation of the climate of 18,000 years BP: Results for the

452   North American/North Atlantic/European sector and comparison with the geologic record of

453   North America, Quaternary Science Reviews, 4, 147-187, 1985.

454   La îné, A., Kageyama, M., Salas-Mélia, D., Voldoire, A., Rivière, G., Ramstein, G., Planton, S.,

455   Tyteca, S., and Peterschmitt, J. Y.: Northern hemisphere storm tracks during the last glacial

456   maximum in the PMIP2 ocean-atmosphere coupled models: energetic study, seasonal cycle,

457   precipitation, Climate Dynamics, 32, 593-614, 2009.

458   Lau, N.-C.: Interactions between Global SST Anomalies and the Midlatitude Atmospheric

459   Circulation, B Am Meteorol Soc, 78, 21-34, 1997.

460   Leathers, D. J., Yarnal, B., and Palecki, M. A.: The Pacific/North American Teleconnection

461   Pattern and United States Climate. Part I: Regional Temperature and Precipitation

462   Associations, Journal of Climate, 4, 517-528, 1991.

463   Li, C. and Battisti, D. S.: Reduced Atlantic Storminess during Last Glacial Maximum: Evidence

464   from a Coupled Climate Model, Journal of Climate, 21, 3561-3579, 2008.

465   Liakka, J.: Interactions between topographically and thermally forced stationary waves:

466   implications for ice-sheet evolution, Tellus A: Dynamic Meteorology and Oceanography,

467   64, 11088, 2012.

468   Liu, Z., Lu, Z., Wen, X., Otto-Bliesner, B. L., Timmermann, A., and Cobb, K. M.: Evolution and

469   forcing mechanisms of El Niño over the past 21,000 years, Nature, 515, 550, 2014.

470   Löfverström, M., Caballero, R., Nilsson, J., and Messori, G.: Stationary Wave Reflection as a

471   Mechanism for Zonalizing the Atlantic Winter Jet at the LGM, Journal of the Atmospheric

472   Sciences, 73, 3329-3342, 2016.

473   Lü, J.-M., Kim, S.-J., Abe-Ouchi, A., Yu, Y., and Ohgaito, R.: Arctic Oscillation during the Mid-

474   Holocene and Last Glacial Maximum from PMIP2 Coupled Model Simulations, Journal of

475   Climate, 23, 3792-3813, 2010.

476   Magnusdottir, G. and Haynes, P. H.: Reflection of Planetary Waves in Three-Dimensional

477   Tropospheric Flows, Journal of the Atmospheric Sciences, 56, 652-670, 1999.

478   Marshall, S. J., James, T. S., and Clarke, G. K.: North American ice sheet reconstructions at the

479   Last Glacial Maximum, Quaternary Science Reviews, 21, 175-192, 2002.

480   Merkel, U., Prange, M., and Schulz, M.: ENSO variability and teleconnections during glacial

481   climates, Quaternary Science Reviews, 29, 86-100, 2010.

Otto-Bliesner, B. L., Brady, E. C., Clauzet, G., Tomas, R., Levis, S., and Kothavala, Z.: Last Glacial Maximum and Holocene Climate in CCSM3, Journal of Climate, 19, 2526-2544, 2006.

Peltier, W. R.: Global glacial isostasy and the surface of the ice-age Earth: The ICE-5G (VM2) model and GRACE, Annual Review of Earth and Planetary Sciences, 32, 111-149, 2004.

Plumb, R. A.: On the Three-Dimensional Propagation of Stationary Waves, Journal of the Atmospheric Sciences, 42, 217-229, 1985.

Rind, D.: Components of the ice age circulation, Journal of Geophysical Research: Atmospheres, 92, 4241-4281, 1987.

Rittenour, T. M., Brigham-Grette, J., and Mann, M. E.: El Niño-Like Climate Teleconnections in New England During the Late Pleistocene, Science, 288, 1039-1042, 2000.

Rivière, G., Laîné, A., Lapeyre, G., Salas-Mélia, D., and Kageyama, M.: Links between Rossby Wave Breaking and the North Atlantic Oscillation–Arctic Oscillation in Present-Day and Last Glacial Maximum Climate Simulations, Journal of Climate, 23, 2987-3008, 2010.

Sherriff-Tadano, S. and Itoh, H.: Teleconnection Patterns Appearing in the Streamfunction Field, SOLA, 9, 115-119, 2013.

Straus, D. M. and Shukla, J.: Does ENSO Force the PNA?, Journal of Climate, 15, 2340-2358, 2002.

Wallace, J. M. and Gutzler, D. S.: Teleconnections in the Geopotential Height Field during the Northern Hemisphere Winter, Monthly Weather Review, 109, 784-812, 1981.

Yanase, W. and Abe-Ouchi, A.: The LGM surface climate and atmospheric circulation over East Asia and the North Pacific in the PMIP2 coupled model simulations, Clim. Past, 3, 439-451, 2007.

505 Yanase, W. and Abe-Ouchi, A.: A Numerical Study on the Atmospheric Circulation over the

506   Midlatitude North Pacific during the Last Glacial Maximum, Journal of Climate, 23, 135-

507   151, 2010.

508 Yeager, S. G., Shields, C. A., Large, W. G., and Hack, J. J.: The Low-Resolution CCSM3,

509   Journal of Climate, 19, 2545-2566, 2006.

510 Zhu, J., Liu, Z., Brady, E., Otto-Bliesner, B., Zhang, J., Noone, D., Tomas, R., Nusbaumer, J.,

511   Wong, T., Jahn, A., and Tabor, C.: Reduced ENSO variability at the LGM revealed by an

512   isotope-enabled Earth system model, Geophysical Research Letters, 44, 6984-6992, 2017.

513